HHS Public Access

Author manuscript

Acta Biomater. Author manuscript; available in PMC 2019 June 01.

Published in final edited form as:

Acta Biomater. 2018 June ; 73: 112–126. doi:10.1016/j.actbio.2018.04.003.

Injectable, porous, biohybrid hydrogels incorporating decellularized tissue components for soft tissue applications

Yang Zhu[1,2], **Sato Hideyoshi**, **Hongbin Jiang**[1], **Yasumoto Matsumura**[1], **Jenna L. Dziki**[1,2], **Samuel T. LoPresti**[1,2], **Luai Huleihel**[1,3], **Gabriela N. F. Faria**[1], **Leah C. Fuhrman**[1], **Ricardo Lodono**[1], **Stephen F. Badylak**[1,2,3], and **William R. Wagner**[1,2,3,4,*]

[1]McGowan Institute for Regenerative Medicine, University of Pittsburgh, Pittsburgh, PA, 15219

[2]Department of Bioengineering, University of Pittsburgh, Pittsburgh, PA, 15219

[3]Department of Surgery, University of Pittsburgh, Pittsburgh, PA, 15219

[4]Department of Chemical Engineering, University of Pittsburgh, Pittsburgh, PA, 15219

Abstract

Biodegradable injectable hydrogels have been extensively studied and evaluated in various medical applications such as for bulking agents, drug delivery reservoirs, temporary barriers, adhesives, and cell delivery matrices. Where injectable hydrogels are intended to facilitate a healing response, it may be desirable to encourage rapid cellular infiltration into the hydrogel volume from the tissue surrounding the injection site. In this study, we developed a platform technique to rapidly form pores in a thermally responsive injectable hydrogel, poly(NIPAAm-co-VP-co-MAPLA) by using mannitol particles as porogens. In a rat hindlimb muscle injection model, hydrogels incorporating porosity had significantly accelerated cellular infiltration. To influence the inflammatory response to the injected hydrogel, enzymatically digested urinary bladder matrix (UBM) was mixed with the solubilized hydrogel. The presence of UBM was associated with greater polarization of the recruited macrophage population to the M2 phenotype, indicating a more constructive foreign body response. The hybrid hydrogel positively affected the wound healing outcomes of defects in rabbit adipose tissue with negligible inflammation and fibrosis, whereas scar formation and chronic inflammation were observed with autotransplantation and in saline injected groups. These results demonstrate the value of combining the effects of promoting cell infiltration and mediating the foreign body response for improved biomaterials options soft tissue defect filling applications.

Graphical abstract

*Corresponding author. McGowan Institute for Regenerative Medicine, University of Pittsburgh, 450, Technology Drive, Pittsburgh, PA 15219, USA. Tel: +1-412-624-5327, Fax: +1-412-624-5363, wagnerwr@upmc.edu.

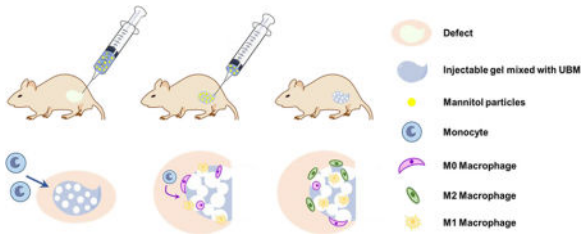

Keywords

hydrogel; porous biomaterial; decellularized extracellular matrix; soft tissue repair; cell infiltration; foreign body response

Introduction

Biodegradable injectable hydrogels have found extensive applications in tissue engineering and a variety of medical procedures, including providing local tissue mechanical support and as vehicles for drug and cell delivery in soft tissue repair [1–6]. One of the advantages of injectable hydrogels is that they can be delivered minimally invasively in a designed, controllable manner [7–9]. In addition, the biodegradability of injectable hydrogels allows tissue regrowth and remodeling. Recently, concepts have been developed to generate porous structure within hydrogels to provide pathways for cell infiltration and tissue integration before hydrogel degradation and collapse [10, 11]. For instance, Griffin et al. employed hydrogel microsphere building blocks to assemble a crosslinked porous scaffold in situ [11]. Bencherif et al. extruded an elastic porous hydrogel through a needle and the subsequent shape recovery opened pores in vivo [10]. A variety of thermally responsive injectable hydrogels have been developed for numerous applications, including to maintain cardiac functions by providing mechanical support to infarcted myocardium upon intramyocardial injection [5, 12–14]. One common family of such thermoresponsive hydrogels are those based on poly(N-isopropylacrylamide) (PNIPAAm), which can be designed to quickly solidify upon warming to body temperature from a low temperature solution. Since these hydrogels collapse into a single phase, they can remain intact at the injection site before degradation with minimal to no signs of cell infiltration into the primary hydrogel mass. As the two previously mentioned methods to form pores in vivo are not compatible with hydrogels having similar rapid in situ gelation mechanisms, there is a need to develop a method to fabricate porous injectable hydrogels. To meet this need, this study evaluated the mixing of mannitol microparticles with poly(NIPAAm-co-VP-co-MAPLA) (VP: N-vinylpyrrolidone, MAPLA: methacrylate-polylactide). In this polymer the pendant hydrophobic MAPLA sidechains generate methacrylic acid units upon hydrolysis, raising the transition temperature and leading to the eventual solubilization of the copolymer, without backbone cleavage [15]). The highly soluble mannitol porogens facilitate the formation of a porous hydrogel shortly after tissue injection.

In addition to supporting cell infiltration and tissue integration, managing the foreign body response is another important and challenging issue. Similar to other implanted medical devices, injectable hydrogels induce foreign body responses, which begin with nonspecific

protein adsorption onto the hydrogel surface and chemoattractant release from platelets and interacting leukocytes [16, 17]. Consequently, these proteins and chemoattractants recruit additional macrophages to the injection sites to interact with the hydrogel surfaces [16, 18–21]. Adherent macrophages are subsequently activated into several heterogeneous phenotypes including classically activated macrophages (M1) which promote inflammation and alternatively activated macrophages (M2) which are involved in tissue remodeling [22]. Modulating macrophage behavior has been put forward as a potential strategy to mediate the foreign body response associated with injectable hydrogels [23].

Decellularized tissue-based materials are comprised of many of the components of the natural extracellular matrices (ECM) from the source tissue. Products derived from such materials have shown strong effects in promoting macrophage polarization towards the M2 phenotype and constructive remodeling in regenerative applications [24–26]. Recent reports have identified matrix-bound vesicles as a principal functional component moderating inflammatory effects in decellularized tissue products [27, 28]. Among the variety of products derived from decellularized tissues, digested formats hold a liquid form at a low temperature which allows thorough mixture with other components, such as with thermally responsive hydrogels. Based on these observations there have been several recent reports that seek to incorporate materials derived from decellularized tissue in the formation of composite materials with improved healing and functional outcomes [29–31].

The overall objective of this study was to develop a fabrication process to create porous injectable hydrogels incorporating decellularized tissue digest material. This new hydrogel material was expected to exhibit faster cellular infiltration and a greater extent of pro-M2 macrophage polarization compared to control groups not incorporating each of the functional components (Scheme 1). Poly(NIPAAm-co-VP-co-MAPLA) was chosen as the representative thermoresponsive hydrogel, and mannitol particles and digested urinary bladder matrix (UBM) were selected as the porogen and the bioactive decellularized material components respectively. A rat hindlimb muscle injection model was employed to characterize in vivo pore formation, cellular infiltration and macrophage polarization functionality. A rabbit adipose tissue defect model was subsequently used to explore the potential of the composite to repair soft tissue defects.

Materials and Methods

Materials

All chemicals were purchased from Sigma-Aldrich unless otherwise stated. N-isopropylacrylamide (NIPAAm) was purified by recrystallization from hexane and vacuum-dried. 2-Hydroxyethyl methacrylate (HEMA) was purified by vacuum distillation. Vinylpyrrolidone (VP), lactide, benzoyl peroxide (BPO), sodium methoxide ($NaOCH_3$), methacryloyl chloride, methacrylic acid (MAA) and other solvents were used as received. D-mannitol particles were sieved to obtain the portion between 170 and 230 meshes.

Synthesis of methacrylate polylactide (MAPLA)

The synthesis of methacrylate polylactide was performed as previously described [32]. Briefly, $NaOCH_3$/methanol was added to a lactide/dichloromethane solution to synthesize polylactide (HO-PLA-OCH_3) through ring-opening polymerization. MAPLA was synthesized by dropping methacryloyl chloride into an HO-PLA-OCH_3/dichloromethane solution containing triethylamine. Dichloromethane was removed by rotary evaporation, and the product was purified by flash chromatography to obtain MAPLA with yields of ~60%.

Synthesis of poly(NIPAAm-co-VP-co-MAPLA) (VP10)

Poly(NIPAAm-co-VP-co-MAPLA) copolymers were synthesized from NIPAAm, VP and MAPLA by free radical polymerization as previously described [7]. The feed ratios of NIPAAm, VP and MAPLA were 80/10/10, and the corresponding product polymers were denoted VP10. Monomers (0.066 mol) were dissolved in 180 mL of 1,4-dioxane containing 0.23 g BPO. The polymerization was carried out at 70°C for 24 h under an argon atmosphere. The copolymer was precipitated in hexane and further purified by precipitation from THF into diethyl ether and vacuum-dried, with yields of ~80%.

Preparation of urinary bladder matrix (UBM) digest

Urinary bladder matrix (UBM) digest was prepared as previously described [33]. Briefly, fresh porcine bladders were obtained (Thoma Meat Market, Pittsburgh, PA) and excess connective tissue and residual urine were removed. The tunica serosa, tunica muscularis externa, the tunica submucosa, and the tunica muscularis mucosa were then mechanically removed. The luminal surface was rinsed with 1.0 N saline solution to dissociate urothelial cells of the tunica. The resulting material was composed of the basement membrane of the urothelial cells plus the subadjacent lamina propria, or UBM. UBM sheets were then placed in a 0.1% (v/v) peracetic acid solution, 4% (v/v) ethanol, and 95.9% (v/v) sterile water for 2 h. To remove peracetic acid, UBM was washed twice for 15 min with PBS followed by two 15 min washes with sterile water. UBM sheets were then lyophilized and the lyophilized UBM was powdered using a Wiley mill and filtered through a 60 mesh screen. The powdered material was solubilized at a concentration of 10 mg/mL in 0.1 mg/mL pepsin in 0.01 N HCl at a constant stir rate of 48 h. The UBM digest solution was then frozen until use in further experiments. The digest was neutralized to a pH of 7.4 using NaOH and diluted in phosphate buffered saline (PBS) to the desired concentration.

Hydrogel preparation

Nonporous hydrogel (NP) was prepared by dissolving VP10 in PBS (10 wt%). Nonporous hydrogel with the UBM digest component (NPE, with “E” denoting the extracellular matrix components from UBM digest) was obtained by mixing 20 wt% VP10 in PBS and 10 mg/mL UBM digest (1:1 v/v). Porous hydrogel without the UBM digest component (PM) was prepared by adding 30 wt% mannitol particles to the NP formula and mixing with a syringe. Pores were formed after PM gelation at 37°C and dissolution of the mannitol particles. Similarly, porous hydrogel with the UBM digest component (PME) was prepared by adding 30 wt% mannitol particles to the NPE formula and mixing with a syringe.

Characterization

Mannitol release from the PM and PME hydrogels were characterized by quantifying the dissolved mannitol in the supernatant of the hydrogel/PBS system. PM or PME hydrogel (0.5 mL) was injected into 10 mL 37°C PBS in 30 s after mixing the hydrogels with mannitol. Supernatants were collected at different time intervals and replaced with fresh 37°C PBS. The mannitol in the supernatants was quantified with a mannitol assay (Sigma-Aldrich, USA) and the cumulative release was calculated accordingly.

Subsequent to 24 h gelation in 37°C PBS, NP, PM and PME hydrogels were frozen in liquid nitrogen, cut to expose the interior and lyophilized. The processed samples were observed by scanning electron microscopy (SEM). The pore sizes of the processed PM and PME hydrogel sections were measured with ImageJ on the micrographs.

To measure the mechanical properties of the hydrogels, samples from the NP, PM and PME groups were incubated in a 37°C water bath for 24 h to reach a stable water content, obtaining hydrogel discs. An ElectroForce 3200 Series II (Bose, Minnesota, US) equipped with a 10 N load cell was utilized to record the compression-force curve immediately after the samples were taken out of the water bath. The compression modulus was calculated from these data for each group.

Hydrogel degradation was quantified by mass loss measurements. Hydrogels with known initial dry masses (~40 mg) were immersed in 4 mL of PBS containing 50 U/mL type I collagenase at 37°C. (Since collagen is one of the major structure proteins in UBM products, in the in vitro degradation test collagenase was added to mimic the in vivo enzymatic degradation mechanism for UBM). At predefined time points over a 4 week period, the hydrogels (n=3 each) were lyophilized and the relative mass loss was recorded.

Cell migration study

Bone marrow-derived macrophages were harvested from 2 month old C57/BL6 mice as previously described [34] using methodology approved by the Institutional Animal Care and Use Committee of the University of Pittsburgh. Briefly, femur and tibiae were harvested and separated from muscle and connective tissue. Bones were cut at either end to expose the bone marrow. Sterile syringe and needles were used to flush out bone marrow using macrophage differentiation media (DMEM/10% FBS/10% L-929 Supernatant/1% PenStrep/2% NEAA/1% HEPES/0.2% β-2 mercaptoethanol). Bone marrow lysate was reconstituted in media and filtered through a sterile cell filter. Cells were plated in 6 well plates and cultured for 7 d in media to differentiate them into macrophages.

NP, PM and PME hydrogels (0.5 mL) were immersed in 10 mL DMEM for 24 h without DMEM replacement. The effect of the released products from NP, PM and PME hydrogels on macrophage migration was evaluated with a CytoSelect cell migration assay (Cell Biolabs, USA) according to the manufacturer's instruction. The releasate (500 μL) was added to the lower well of the migration plate. 150,000 macrophages were added to the inside of each insert (n=4 each group). DMEM only was used as control.

Rat hind limb hydrogel injection studies

Adult female Lewis rats weighing 160−210 g were utilized in a protocol that was approved by the University of Pittsburgh's Institutional Animal Care and Use Committee. Anesthesia was induced with 3.0% isoflurane inhalation with 100% oxygen followed by 1.5-2% isoflurane with 100% oxygen during the procedure. Dermatotomy was performed to expose the inner thigh muscles on both legs. Single injections of 200-250 uL of hydrogel were made approximately 3 mm deep in the muscle bed. For each hydrogel, 18 injections in 18 legs were made. For acute studies, the inner thigh muscles from 2 legs each of NP, PM and PME group were excised 3 min after injection. The muscles were incised to expose the hydrogel injection site, and images were taken with a Dino-Lite (AM4113T-GFBW, AnMo Electronics, New Taipei City, Taiwan) under brightfield mode. For longer term studies, after 3 and 21 d, 4 rats from each group at each time point were sacrificed and the inner thigh muscles encompassing the hydrogel injection site were excised, and the tissue was fixed in 10% formaldehyde for 3 d before embedding. Trichrome and immunohistochemical staining with monoclonal antibodies against CD68 (1:200, Abcam, USA), CD86 (1:150, Abcam, USA) and CD206 (1:200, Santa Cruz, USA) were performed. CD68 was co-stained with CD86 and CD206 separately. A red secondary antibody was used for CD68, green secondary antibodies were used for CD86 and CD206. Nuclei were stained with 40',6-diamidino-2-phenylindole (DAPI; 1:10000, Sigma). Microscopic images were taken byr fluorescence microscopy.

Cell densities around and in the hydrogel injection sites for each group at day 3 and day 21 were analyzed from the microscopic images using ImageJ. M1 macrophages were identified by CellProfiler as $CD68^+/CD86^+$/DAPI cells. M2 macrophages were identified by CellProfiler as $CD68^+/CD206^+$/DAPI cells.

Rabbit adipose tissue defect repair

Female New Zealand rabbits (5 months old, 3.5 kg) were utilized in a protocol that followed the National Institutes of Health guidelines for animal care that was approved by the University of Pittsburgh's Institutional Animal Care and Use Committee. Anesthesia was induced with ketamine/xylazine and maintained with inhalant isoflurane via nose cone. Dermatotomy was performed to expose the inner thigh adipose tissues on both legs. For the sham group, the wound in the skin was closed 5 min after dermatotomy. For the PBS, fat transplantation and PME gel groups, a 1 × 1 cm defect was created by removing a section of the fat pad in the center of the adipose tissues. The defect site was marked for identification purposes during explantation with non-absorbable sutures in the corners. For the fat transplantation group, adipose tissue removed from the other leg of the same animal was placed in the defect and sutured to surrounding fat tissue followed by wound closure. For the PBS group, 1 mL PBS was injected into the defect after closing the skin wound. Similarly, 1 mL PME hydrogel was injected into the defect after closing the skin wound for the PME Gel group. Experiments were designed so that different treatments were made in the same rabbit.

At 2 and 8 wk after surgery, the surgical sites were examined by palpatation by the same clinician to compare the stiffness of the underlying tissue with the healthy control group (Since Dr. Sato was the only one who has experience of using this technique in patients, he

is the only one who scaled the tissues). The perceived tissue stiffness was scored on a 1 to 5 scale with 1 being the most soft and 5 being the most stiff. The rabbits were then sacrificed, and the inner thigh adipose tissue encompassing the defects was excised. The tissue was fixed in 10% formaldehyde for 3 d before embedding. Trichrome staining and Oil Red staining were performed on paraffin sections and frozen sections, respectively. Adipocyte size and density of crown-like structures were analyzed by ImageJ. Isolectin/BIOPSY/DAPI staining was performed on the frozen sections.

Statistical analyses

For paired comparisons, a t-test was employed. Where three or more groups were being compared, one-way ANOVA was employed with Tukey's test applied for specific comparisons. Results are presented as the mean with standard deviation. Kruskal-Wallis and Mann-Whitney test (non-parametric) were used to evaluate the differences among scored tissue stiffness. Statistical significance was defined as $p < 0.05$.

Results

Porous hydrogel formation

As shown in Figure S1, sieved mannitol particles have an initial size of 68.0 μm. After mixing with the VP10 hydrogel solution for 10 min, the particle size did not decrease significantly. In addition, there was no size difference between particles mixed with or without UBM digest in the hydrogel. After injecting the hydrogel/mannitol mixtures into 37°C PBS, the mixtures instantly solidified, and mannitol was rapidly dissolved and released from the hydrogel mass. After 24 h, 80% of the mannitol was released from the hydrogel of PM group, whereas 100% of the mannitol was released from the hydrogel of PME group, as shown in Figure S2a.

Densely packed pores can be observed in the hydrogels of PM and PME groups after 24 h of gelation, as opposed to the nonporous hydrogel mass of the NP group (Figure 1). The majority of the pores found in PM and PME groups were elliptical. The pore size of PM group was 237±80 μm, significantly smaller than the pore size of PME group, which was 295±87 μm (Figure S2b). In addition, channels wider than 50 μm could be observed on the walls of the pores, creating interconnected pores (Figure 1).

Release of UBM component

Matrix-bound vesicles (MBVs) were found by Transmission electron microscope (TEM) in the supernatant 2 min after hydrogel immersion in 37°C PBS, as shown in Figure S3a. The MBVs showed a typical size as previously reported and remained intact [27]. The protein content of UBM mixed in the hydrogel was rapidly released. 48% of the total protein was released within 30 min of gelation, 70% was released after 24 h gelation (Figure S3c).

Physical properties of porous hydrogel

The compression modulus of the nonporous hydrogel (NP group) was 272±38 kPa. Pore structures significantly decreased the compression modulus to 106±8 kPa and 87±6 kPa for PM group and PME group, respectively (Figure 2a). There was no difference in terms of

degradation rate, hydrogel of PME group lost weight in PBS faster than NP and PM groups. As shown in Figure 2b, PME hydrogel lost 50% weight in 2 weeks in collagenase/PBS, while similar weight loss took 3 weeks for the other two groups.

Influence of hydrogel on cell behaviors

Dissolved mannitol did not show cytotoxicity on SMCs up to 100 mM, as shown in Figure S4. Compared to SMCs treated with PBS, SMCs treated with products released from the hydrogels did not impact proliferation over a week (Figure S3b). SMCs significantly proliferated during the culture period, as indicated by mitochondrial activity assay and visual inspection, but neither mannitol, proteins, MBVs nor other components promoted or inhibited cell proliferation over this period (Figure S4b). On the other hand, the released products from the PME hydrogel attracted macrophages to migrate through 8 μm membrane towards the high concentration source, as shown in Figure 3. Released products from the other two groups did not show a significant effect on macrophage migration compared to the PBS group (Figure 3).

Cell infiltration into hydrogel in vivo

Immediately after injection into the rat hindlimb, hydrogel from all three groups solidified and formed a hydrogel mass in the muscle bed as a result of temperature increase. As shown in Figure 4, clear boundaries could be identified between the hydrogels and the muscle. For the hydrogel from the NP group, hydrogel mass was continuous and homogeneous, whereas pores can be found in injected PM and PME hydrogels (pointed by arrows in Figure 4). In addition, similar to the in vitro result, channels between pores could be found in the PM and PME hydrogels.

Three days after injection, rat leg muscles with injected hydrogel were sectioned and stained. On DAPI stained images, hydrogel injection sites could be identified in all three groups. In NP and PM groups, empty regions were apparent on the tissue sections that were devoid of cell nuclei, corresponding to the region in which the hydrogels had been injected. These regions were encompassed by a capsule ~100 μm thick of densely packed cells (Figure 5). A similar capsule of cells was found around the injected hydrogel in the PME group. However, in contrast to the other two groups, cells were present in the hydrogel area, at a lower density compared to the cell density in the capsule. Of note, the entire hydrogel injection site was not infiltrated by cells. Rather, the core of the PME hydrogels remained cell-free 3 d after injection. As for the NPE group (non-porous VP10 hydrogel mixed with UBM digest), cells were observed to be further in the hydrogel from the hydrogel/capsule edge (Figure S5). However, the cells did not penetrate as far as in the PME group.

Twenty-one days after injection, the capsules surrounding the injection sites for all three groups did not show obvious changes regarding thickness or cell density compared to the capsules at day 3, as shown in Figure 5c. For the two groups that did not show cell infiltration at day 3, no signs of cell infiltration in the NP group appeared given another 18 days, as opposed to the extensive infiltration towards the core of the injected hydrogel observed in the PM group. Similar to the NP group at day 3, the core of the PM hydrogel was not occupied by cells at day 21 (Figure 5c). On the other hand, the entire injection site

of the PME group was filled with cells, including the core of the hydrogel. As shown in Figure 5c, the cells evenly distributed in the injection area, and the density of the infiltrated cells was significantly higher than the density of cells in the hydrogel area of the PM group. In addition, compared to day 3, the cell density in the injection area of the PME group at day 21 increased (Figure 5f). Echoing the cell infiltration results, no extracellular matrix deposition was visually apparent at day 21 in the NP hydrogel injection area, while extensive extracellular matrix deposition was seen in sections from the PM and PME groups (Figure 5d).

Macrophage polarization

Cells around and in the injection areas stained positively with macrophage markers. CD68 (red)/CD86 (green) and CD68 (red)/CD206 (green) were stained on separate sections. As shown in Figure 6a-d, $CD68^+$ cells were present in, concentrated in and comprised the major portion of the cell red fluorescence from CD68 population in the capsule around the injection areas for all three groups at day 3. Colocalization of the and green fluorescence from CD86 was observed in all three groups, resulting in yellow cells in the capsules (Figure 6a,c). The $CD68^+/CD86^+$ subgroups of macrophages ($CD68^+$ cells) were evenly distributed in the capsules without preference on either the hydrogel side or the muscle side. Quantitative results given by CellProfiler showed that around 60% of the macrophages were CD86 positive for all three groups at day 3 (Figure 6e). $CD68^+/CD206^+$ subgroups of macrophages were also identified in the capsules (Figure 6b,d). Similar to the $CD86^+$ macrophages, $CD206^+$ macrophages distributed evenly in the capsules. For NP, PM, and PME, 35%, 40% and 55% of the macrophages were $CD206^+$, respectively (Figure 6f). However, no significant differences among the $CD206^+$ percentages were identified. Further calculation showed that the ratio between $CD206^+$ macrophages and $CD86^+$ macrophages for the NP group (57%) was smaller than for the PME group (90%) group (Figure 6g), indicating that the macrophages in the capsules around injected NP hydrogel were polarized more toward an M1 phenotype compared to the PME group. No differences were found between the NP and PM groups, or between PM and PME groups. Since no cells had infiltrated the NP and PM hydrogels at day 3, only the infiltrating macrophage polarization for the PME group was analyzed. Compared to macrophages in the capsule, macrophages in the PME hydrogel were less polarized, as both the $CD86^+$ and $CD206^+$ percentages were smaller (Figure 6e,f). However, the ratio between $CD206^+$ macrophages and $CD86^+$ macrophages was not different from the ratio of the macrophages in the capsule (Figure 6g).

At day 21, the foreign body response did not diminish, with macrophages remaining around and within the injection sites, as shown in Figure 7a,b. CD68 staining showed cells infiltrating the PM hydrogel and that the cells following the first wave of infiltration in the PME hydrogel were mostly macrophages (Figure 7a,b). Similar to the results at day 3, colocalization of CD68 and CD86 was observed for a significant portion of the macrophages in the capsules for all three groups (Figure 7a,c). The percentage of $CD86^+$ macrophages decreased significantly between day 3 (61%) and day 21 (53%) for the PME group, while the percentages did not change significantly for NP and PM groups (Figure 7e). In terms of the $CD206^+$ subgroup of macrophages in the capsules, the percentages decreased significantly between day 3 (40% and 55%) and day 21 (17% and 43%) for PM and PME

groups respectively, while no significant changes were found for the NP group (Figure 7f). From day 3 to day 21, the ratio between $CD206^+$ macrophages and $CD86^+$ macrophages in the capsules for the PM group decreased significantly, while the ratios for the NP and PME groups remained at the same level (Figure 7f). As a result, the PME group showed the highest $CD206^+/CD86^+$ ratio among the three groups, and the ratio for the NP group was higher than for the PM group. In terms of the $CD206^+/CD86^+$ ratio, the macrophages infiltrating the PM hydrogel appeared to be more polarized toward the M1 phenotype compared to the macrophages in the capsule around the PM hydrogel and the macrophages infiltrating the PME hydrogel (Figure 7g).

Repair of adipose tissue defect

Two weeks after surgery, adipose tissue samples collected from rabbits in the Sham group showed structures resembling that of healthy adipose tissue, featuring densely packed hexagonal adipocytes (Figure 8a). In contrast, for the PBS injection group, the defect wounds closed and were infiltrated by scar tissue. Inflammation could be found in adipose tissue adjacent to the scar: the organized structure of adipocytes was disrupted by inflammatory cell infiltration and collagen deposition. Similar to the PBS group, inflammation was observed in and around transplanted autologous fat, especially along the boundary of the tissue bed and the implanted tissue. In comparison, adipose tissue near the defect filled with PME hydrogel maintained the morphology of healthy fat tissue. A thick layer of cells attributed to the foreign body response encompassed the injected PME hydrogel, comparable to the phenomenon found in the rat model (hydrogel mass could be observed during the excision procedure). As shown in Figure 8, there was extensive cellular penetration across the hydrogel-tissue interface and infiltrating the porous hydrogel, consistent with previous findings, yet at this time point there was not morphological evidence of new adipose tissue in the hydrogel pocket. Oil Red staining supported the observations made from the trichrome staining. Oil droplets occupied almost all of the volume in the adipocytes and the volume of the adipose tissue. This characteristic of normal adipose tissue was also present in fat tissue around the implanted hydrogel. In contrast, oil droplets in the PBS group and Fat Transplantation group lost their normal morphology, with smaller, disjointed areas staining positively with Oil Red. These stained areas were discontinuous compared to those in the Sham and PME Gel groups.

At 8 weeks post-surgery, the gross appearance of the treated adipose tissue in the animals is shown in Figure 9. Unlike the 2 week time point, no hydrogel mass was found in the PME hydrogel treated group. Despite migration and tissue encapsulation, more than half of the suture markers could be located after 8 weeks and were generally found to have maintained the square layout created at the time of intervention (Figure 9). The distances between the markers in the PBS group appeared to have decreased as the defects closed, whereas the marker patterns in the Fat Transplantation group and PME Hydrogel group did not appear to shrink. Due to the loss of some of the markers and the limited numbers of rabbits in each group, this observation was necessarily qualitative. Tactile semi-quantitative evaluation of the treated areas prior to re-opening of the surgical site revealed that the tissue for the Fat Transplantation group, but not the other groups, became stiffer (stiffness score increased from 1.8±0.3 to 2.8±0.3 in the Fat Transplantation group). Further qualitative examination of

the tissue surrounding the surgical areas indicated that these tissues did not stiffen for any of the groups. The stiffening of the fat transplanted site was consistent with the extensive chronic inflammation and fibrotic tissue deposition found histologically in the Fat Transplantation group (Figure 10). Mild inflammation was observed near the scar formed in the defect of the PBS group, which appeared to have dissipated from the acute inflammation found at 2 weeks post-surgery. Tissue collected from the Sham and PME Gel groups exhibited little morphological differences compared to the healthy control tissue, showing negligible signs of inflammation or fibrosis (Figure 10). Oil Red staining reflected the observations made with trichrome staining. The organization of adipocytes in the Sham, PME Gel, and PBS groups (besides the scar tissue apparent in the latter group) resembled that of the Healthy group, while adipocytes in the Fat Transplantation group were interspersed with fibrotic tissue. Isolectin staining (red channel in the right column of Figure 10) highlighted vascular structures and macrophages within the treated adipose tissue. PME Gel treated adipose tissue generally presented a vascular morphology similar to that of the Sham and Healthy groups. Putative macrophages were apparent in sites treated with the transplanted fat tissue, co-localizing with fibrotic tissue and making it difficult to discern the vasculature. A high density of macrophages was also found in the scar and at the interface of the scar and healthy adipose tissue in tissues in the PBS group.

Adipocyte size is a reflection of the status of the cells, which is influenced by metabolic activities, inflammation, and fibrosis of the adipose tissue [35]. In terms of cell area in tissue cross-section, the adipocyte size distribution for healthy fat presented a single peak distribution, with the most frequent area being between 4000 and 5000 μm^2 (Figure 11). For the Sham group 8 weeks after surgery, a subpopulation of the adipocytes became larger, with the primary peak area being comparable to healthy tissue. For the three types of treated defects, the peaks of the area distribution shifted smaller with each showing the highest frequency between 1000 and 2000 μm^2. The size distribution for the PBS group showed a single, narrow peak, while the distribution for the PME Gel group was skewed with a tail of larger adipocytes. Distinct from other groups, the adipocyte area distribution for the Fat Transplantation group had a longer tail in the larger area region; a significant subgroup of the adipocytes being larger than 15000 μm^2. On average, adipocytes in the Fat Transplantation group were larger than for all other groups (Figure 11b), whereas the cells were smaller in the PBS treated tissue. Adipocytes from the PME Gel treated tissue had a similar average area compared to the Healthy and Sham groups. Looking at another morphological parameter, the number of crown-like structures were quantified for all groups. This parameter, related to apoptotic activity [36], was found to be markedly elevated for the Fat Transplantation group.

Discussion

There is an increasing need for biomaterial-based soft tissue fillers for patients who have congenital soft tissue defects, traumatic injuries, surgical resections and cosmetic needs. Mechanical properties, degradation profile, and cell/tissue interaction including tissue integration and vascularization are the primary considerations in developing desirable biomaterial options for soft tissue applications. Hydrogels, especially those derived from natural sources have the advantage of high bioactivity and mechanical properties that may

approximate target tissue in addition to the potential for injection-based delivery. Porous scaffolds, generally not delivered by injection, have the desirable features of increased tissue integration and vascularization potential. Although not optimized, the porous injectable hydrogel described in this work combined the desirable features from these two general types of soft tissue fillers.

For most injectable hydrogel designs, the integration of the injected hydrogels and the host tissue is highly dependent on the degradation of the hydrogel mass. Slow hydrogel degradation may result in minimal tissue ingrowth and result in prolonged undesired material-tissue interaction leading to material encapsulation. Fast hydrogel degradation could lead to failure in mechanical support and quick erosion from the void space into which cell infiltration is desired [11, 37]. Efforts have been made to match the degradation rates of hydrogels to the temporal requirements to achieve maximal beneficial effects. As hydrogels usually form nonporous crosslinked swollen masses upon injection, one strategy is to incorporate enzyme cleavable sites to allow cells to actively migrate into the hydrogels [38, 39]. Another strategy is to tune hydrogel degradation rate by controlling the crosslinking density or hydrolytical potential [15, 40].

Recently developed porous hydrogels have been shown to encourage cell infiltration into the hydrogel prior to significant mass loss [11, 41, 42]. However, the adaptability of those strategies to gels employing rapid in situ gelation mechanisms is limited. Sacrificial porogen leaching has been extensively adopted in fabricating porous scaffolds with control over pore size, porosity and connectivity [43–46]. In principle, porogen leaching is compatible with various gelation mechanisms and material candidates to obtain corresponding combinations for injectable porous hydrogels. The key is the coordination of delivery time, gelation time and dissolution time of the porogen. In this study, mannitol was chosen not only for its cytocompatibility and clinical use as a tissue injectate [47, 48], but also its solubility characteristics. Mannitol is highly soluble in saline at body temperature, while its solubility is relative low at 4°C. This behavior is opposite of that for poly(NIPAAm-co-VP-co-MAPLA) in PBS solution. Due to the contrasting solubility characteristics, a mixture of hydrogel solution and mannitol particles was feasible at 4°C, with an insignificant decrease in particle size, and rapid dissolution initiated at approximately the same time of the thermally-induced phase transition for the hydrogel. Porogens with higher solubility may have dissolved during the mixing and injection steps, or during sol-gel transition for hydrogels with slower gelling mechanisms. On the other hand, slightly soluble porogens or porogens with slow dissolving rates may not generate porous structures shortly after gelation for subsequent cell infiltration (for instance, gelatin microspheres did not dissolve 24 h after gelation of poly(NIPAAm-co-VP-co-MAPLA) hydrogel, data not shown). In addition, the porogens should not interfere with the gelation process or the resultant crosslinks. As a variety of other injectable hydrogels employ rapid, in situ gelation mechanisms, and since it is in principle easy and convenient to mix the porogen (and digested ECM) with hydrogel precursors prior to injection, it appears that the described technique would be readily transferred to a wide spectrum of injectable hydrogels.

An unexpected finding was that the measured pore sizes in the collapsed hydrogels were significantly greater than the size of the loaded mannitol particles, and that channels were

formed connecting adjacent pores. Compared to the original design in which the walls between pores were thin to allow channel formation upon degradation, the existing connections formed during mannitol dissolution would theoretically be more beneficial for cell infiltration. It is speculated that there was a short range fluctuation in mannitol particle concentration during the mixing and gelation steps which resulted in local aggregation of particles by the end of the gelation. Since the volume of hydrogel solution between aggregated particles would be minimal, internal structures within the larger pores would not be stable. The channels between pores may be due to particle aggregates contacting each other during hydrogel gelation. Although the focus of this study was to demonstrate the concept of fabricating porous injectable hydrogels (in combination with modulating the foreign body response), learning the mechanism behind this phenomenon and understanding the relationship between particle size/concentration and pore structure in order to design and control pore structure is of value for further investigation.

In addition to promoting cell infiltration, the polarization of macrophages towards a remodeling phenotype has been achieved. The foreign body response induced by injectable hydrogels have been an obstacle in achieving more favorable therapeutic outcomes. Current strategies of moderating the classic foreign body response are emphasizing reduction in macrophage activation. Vegas et al. identified that triazole modified alginate hydrogel inhibited recognition by macrophages and fibrous deposition among a library of modified alginate hydrogels, although the mechanism is not clear [49]. Zhang et al. employed the superhydrophilicity of zwitterionic polymers to form nondegradable hydrogels with low protein adsorption levels as a means to reduce macrophage activation [17]. In addition to less dense collagen deposition, a movement of macrophage polarization toward an M2 phenotype on zwitterionic hydrogels compared to control materials was found. However, making a material “invisible” does not take advantage of the potential constructive effects of the macrophages [17, 49]. In this study, macrophage infiltration was not discouraged, but M2 polarization of recruited macrophages was putatively enhanced by the inclusion of ECM digest. Previous studies and reviews showed not only the desirability but the necessity for a macrophage transition from proinflammatory, M1 phenotype to the constructive and modulatory M2 phenotype for constructive and functional healing and regeneration in various body systems including muscle, heart, skin, urogenital tract, and central nervous system, among others [50–55]. In a recent mechanistic study by Huleihel et al. MBVs have been identified as one of the most decisive components in ECM products in terms of the corresponding bioactivities [27]. Therefore, the introduced simple strategy is theoretically widely applicable to other injectable hydrogel materials, as has been presented in other types of biomaterials and devices [29, 56, 57].

In this study, UBM was added to the hydrogel and applied in muscle and adipose tissue models. Homologous (same tissue) versus heterologous (different tissue from the intended use) source tissue ECM as the preferred material for given applications has been well studied. In a recent study of ECM use for volumetric muscle loss in 14 human patients, no detectable difference was seen between dermal ECM, small intestinal submucosa derived ECM or UBM[58]. In a study comparing ECM effects upon neuronal stem cell differentiation, UBM-ECM was shown to be superior to brain ECM [59]. In contrast, homologous sources were shown to be superior in models involving other anatomic sites of

corresponding clinical applications. However, whether UBM is the most suitable choice for use in adipose tissue is yet to be determined.

The in vivo results achieved with ECM component inclusion were generally encouraging, and associated with these results, several influential factors and accompanying effects should be discussed. The UBM product promoted cell infiltration, thus increasing the number of macrophages in and around the hydrogel. Although the overall pro-M2 polarization effect has been demonstrated, the population of M1-like macrophages enlarged as well. The impact of such an effect on specific applications would need to be evaluated. In addition, pore size (curvature) has been shown to affect macrophage polarization in polyester scaffolds, indicating there may be a favorable range of pore sizes [60]. The diameter of mannitol particles was originally chosen according to the pore size reported to be associated with pro-M2 phenotype behavior in previous studies [60]. As the concept of modulating macrophage polarization has been shown, in this study the authors did not attempt to optimize the pore size, and in fact the observed pores were larger than expected. Porosity (theoretically mainly affected by the wt% of mannitol mixed into gel) was not optimized, as well, which is another limitation of this study as it may affect the cell infiltration rate and modulus of hydrogel. The hydrogel compressive modulus was also affected by mixing in ECM. Blakney et al. studied activation of macrophages on poly(ethylene glycol)-based hydrogels with compressive moduli of 130, 240 and 840 kPa and found that hydrogels with lower stiffness led to reduced macrophage activation [61]. Since the PME gel was porous, the compression modulus of the hydrogel substrate was higher than the composite. Comparing the stiffness of the PM and PME gels, the compression modulus of substrate in the PME gel was estimated to be between 200 and 250 kPa. Therefore, mechanical property influence on pro-M2 macrophage polarization might be further improved by optimizing the stiffness of the hydrogel substrate. The effect of hydrogel degradation rate was also not directly examined. Since ECM component addition was associated with faster degradation, it is not possible to separate these effects.

Some further limitations associated with the in vivo studies should be noted. The macrophage polarization and adipose tissue repair were done in different species and in different tissue beds. The rat was convenient for the general muscle injection study since there are a variety of specific antibodies available with the rat model to characterize the biological response. The rat also represents a lower animal than the rabbit for this first level study. However, for a more clinically relevant model where a soft tissue defect is present, the rabbit was utilized since it provided an adequately sized fatty tissue depot. Unfortunately, fewer monoclonal antibodies are available for the rabbit model, limiting the characterization to more morphology-based assessments. In addition, this study employed only one pair of M1 and M2 markers to support the identification of macrophage phenotype. The use of further markers may have provided stronger confirmation of the observed results for this parameter. Finally, as we propose the concepts and methods of introducing porous structures in injectable hydrogels and encouraging constructive foreign body responses for hydrogels, the utilities of these concepts and methods in promoting soft tissue regeneration and other soft tissue applications in addition to the wound healing function demonstrated in this study are yet to be evaluated.

Conclusion

In this study, a fabrication process to create porous injectable hydrogels incorporating decellularized tissue digest was developed. Poly(NIPAAm-co-VP-co-MAPLA) was chosen as a representative fast gelling thermoresponsive hydrogel, and mannitol particles and digested urinary bladder matrix were selected as the porogen and bioactive decellularized tissue components respectively. Connective porous structures with desirable pore sizes were formed in situ upon injection. In soft tissue injection models, this new hydrogel material induced more rapid cellular infiltration and a greater extent of M2 macrophage polarization compared to control groups not incorporating all of the functional components. The combined strategy of pore formation in injectable hydrogels together with the provision of ECM-based components to mediate the foreign body response toward a more constructive outcome should be transferrable to a variety of other injectable hydrogel systems for soft tissue applications.

Supplementary Material

Refer to Web version on PubMed Central for supplementary material.

Acknowledgments

The financial support for this work by the US National Institutes of Health (grant R01 HL105911) and Commonwealth of Pennsylvania is gratefully acknowledged.

References

1. Ko DY, Shinde UP, Yeon B, Jeong B. Recent progress of in situ formed gels for biomedical applications. Prog Polym Sci. 2012
2. He C, Kim SW, Lee DS. In situ gelling stimuli-sensitive block copolymer hydrogels for drug delivery. J Control Release. 2008:189–207. [PubMed: 18321604]
3. Dou QQ, Liow SS, Ye E, Lakshminarayanan R, Loh XJ. Biodegradable Thermogelling Polymers: Working Towards Clinical Applications. Adv Healthc Mater. 2014 n/a-n/a.
4. Miao B, Song C, Ma G. Injectable thermosensitive hydrogels for intra-articular delivery of methotrexate. J Appl Polym Sci. 2011:2139–2145.
5. Yoshizumi T, Zhu Y, Jiang H, D'Amore A, Sakaguchi H, Tchao J, Tobita K, Wagner WR. Timing effect of intramyocardial hydrogel injection for positively impacting left ventricular remodeling after myocardial infarction. Biomaterials. 2016:182–193.
6. Li J, Darabi M, Gu J, Shi J, Xue J, Huang L, Liu Y, Zhang L, Liu N, Zhong W, Zhang L, Xing M, Zhang L. A drug delivery hydrogel system based on activin B for Parkinson's disease. Biomaterials. 2016:72–86.
7. Zhu Y, Wood NA, Fok K, Yoshizumi T, Park DW, Jiang H, Schwartzman DS, Zenati MA, Uchibori T, Wagner WR, Riviere CN. Design of a Coupled Thermoresponsive Hydrogel and Robotic System for Postinfarct Biomaterial Injection Therapy. Ann Thorac Surg. 2016:780–786.
8. Seif-Naraghi SB, Singelyn JM, Salvatore MA, Osborn KG, Wang JJ, Sampat U, Kwan OL, Strachan GM, Wong J, Schup-Magoffin PJ, Braden RL, Bartels K, DeQuach JA, Preul M, Kinsey AM, DeMaria AN, Dib N, Christman KL. Safety and efficacy of an injectable extracellular matrix hydrogel for treating myocardial infarction. Sci Transl Med. 2013:173ra125.
9. Martinez-Sanz E, Ossipov DA, Hilborn J, Larsson S, Jonsson KB, Varghese OP. Bone reservoir: Injectable hyaluronic acid hydrogel for minimal invasive bone augmentation. J Control Release. 2011:232–240.

10. Bencherif SA, Sands RW, Bhatta D, Arany P, Verbeke CS, Edwards DA, Mooney DJ. Injectable preformed scaffolds with shape-memory properties. Proc Natl Acad Sci U S A. 2012:19590–19595. [PubMed: 23150549]
11. Griffin DR, Weaver WM, Scumpia PO, Di Carlo D, Segura T. Accelerated wound healing by injectable microporous gel scaffolds assembled from annealed building blocks. Nat Mater. 2015:737–744. [PubMed: 26030305]
12. Fujimoto KL, Ma Z, Nelson DM, Hashizume R, Guan J, Tobita K, Wagner WR. Synthesis, characterization and therapeutic efficacy of a biodegradable, thermoresponsive hydrogel designed for application in chronic infarcted myocardium. Biomaterials. 2009:4357–4368. [PubMed: 19487021]
13. Cui Z, Lee BH, Pauken C, Vernon BL. Degradation, cytotoxicity, and biocompatibility of NIPAAm-based thermosensitive, injectable, and bioresorbable polymer hydrogels. J Biomed Mater Res A. 2011:159–166. [PubMed: 21548065]
14. Garbern JC, Hoffman AS, Stayton PS. Injectable pH- and temperature-responsive poly(N-isopropylacrylamide-co-propylacrylic acid) copolymers for delivery of angiogenic growth factors. Biomacromolecules. 2010:1833–1839. [PubMed: 20509687]
15. Zhu Y, Jiang H, Ye SH, Yoshizumi T, Wagner WR. Tailoring the degradation rates of thermally responsive hydrogels designed for soft tissue injection by varying the autocatalytic potential. Biomaterials. 2015:484–493.
16. Anderson JM, Rodriguez A, Chang DT. Foreign body reaction to biomaterials. Semin Immunol. 2008:86–100. [PubMed: 18162407]
17. Zhang L, Cao Z, Bai T, Carr L, Ella-Menye JR, Irvin C, Ratner BD, Jiang S. Zwitterionic hydrogels implanted in mice resist the foreign-body reaction. Nat Biotechnol. 2013:553–556. [PubMed: 23666011]
18. Broughton G II, Janis JE, Attinger CE. The Basic Science of Wound Healing. Plast Reconstr Surg. 2006
19. Tang L, Jennings TA, Eaton JW. Mast cells mediate acute inflammatory responses to implanted biomaterials. Proc Natl Acad Sci U S A. 1998:8841–8846. [PubMed: 9671766]
20. Rhodes NP, Hunt JA, Williams DF. Macrophage subpopulation differentiation by stimulation with biomaterials. J Biomed Mater Res. 1997:481–488. [PubMed: 9407296]
21. Charo IF, Ransohoff RM. The Many Roles of Chemokines and Chemokine Receptors in Inflammation. New Engl J Med. 2006:610–621. [PubMed: 16467548]
22. Sridharan R, Cameron AR, Kelly DJ, Kearney CJ, O'Brien FJ. Biomaterial based modulation of macrophage polarization: a review and suggested design principles. Mater Today. 2015:313–325.
23. Meng FW, Slivka PF, Dearth CL, Badylak SF. Solubilized extracellular matrix from brain and urinary bladder elicits distinct functional and phenotypic responses in macrophages. Biomaterials. 2015:131–140.
24. Brown BN, Ratner BD, Goodman SB, Amar S, Badylak SF. Macrophage polarization: an opportunity for improved outcomes in biomaterials and regenerative medicine. Biomaterials. 2012:3792–3802. [PubMed: 22386919]
25. Badylak SF, Freytes DO, Gilbert TW. Reprint of: Extracellular matrix as a biological scaffold material: Structure and function. Acta Biomater. 2015:S17–26. [PubMed: 26235342]
26. Huleihel L, Dziki JL, Bartolacci JG, Rausch T, Scarritt ME, Cramer MC, Vorobyov T, LoPresti ST, Swineheart IT, White LJ, Brown BN, Badylak SF. Macrophage phenotype in response to ECM bioscaffolds. Semin Immunol. 2017:2–13. [PubMed: 28736160]
27. Huleihel L, Hussey GS, Naranjo JD, Zhang L, Dziki JL, Turner NJ, Stolz DB, Badylak SF. Matrix-bound nanovesicles within ECM bioscaffolds. Science Advances. 2016
28. Huleihel L, Bartolacci JG, Dziki JL, Vorobyov T, Arnold B, Scarritt ME, Pineda Molina C, LoPresti ST, Brown BN, Naranjo JD, Badylak SF. Matrix-Bound Nanovesicles Recapitulate Extracellular Matrix Effects on Macrophage Phenotype. Tissue Eng Part A. 2017:1283–1294. [PubMed: 28580875]
29. Hachim D, LoPresti ST, Yates CC, Brown BN. Shifts in macrophage phenotype at the biomaterial interface via IL-4 eluting coatings are associated with improved implant integration. Biomaterials. 2017:95–107.

30. Hussey GS, Keane TJ, Badylak SF. The extracellular matrix of the gastrointestinal tract: a regenerative medicine platform. Nature Reviews Gastroenterology & Hepatology. 2017:540. [PubMed: 28698662]
31. Wolf MT, Carruthers CA, Dearth CL, Crapo PM, Huber A, Burnsed OA, Londono R, Johnson SA, Daly KA, Stahl EC, Freund JM, Medberry CJ, Carey LE, Nieponice A, Amoroso NJ, Badylak SF. Polypropylene surgical mesh coated with extracellular matrix mitigates the host foreign body response. J Biomed Mater Res A. 2014:234–246. [PubMed: 23873846]
32. Ma Z, Nelson DM, Hong Y, Wagner WR. Thermally responsive injectable hydrogel incorporating methacrylate-polylactide for hydrolytic lability. Biomacromolecules. 2010:1873–1881. [PubMed: 20575552]
33. Freytes DO, Martin J, Velankar SS, Lee AS, Badylak SF. Preparation and rheological characterization of a gel form of the porcine urinary bladder matrix. Biomaterials. 2008:1630–1637. [PubMed: 18201760]
34. Sicari BM, Dziki JL, Siu BF, Medberry CJ, Dearth CL, Badylak SF. The promotion of a constructive macrophage phenotype by solubilized extracellular matrix. Biomaterials. 2014:8605–8612. [PubMed: 25043569]
35. Divoux A, Tordjman J, Lacasa D, Veyrie N, Hugol D, Aissat A, Basdevant A, Guerre-Millo M, Poitou C, Zucker JD, Bedossa P, Clement K. Fibrosis in human adipose tissue: composition, distribution, and link with lipid metabolism and fat mass loss. Diabetes. 2010:2817–2825. [PubMed: 20713683]
36. Mancuso P. The role of adipokines in chronic inflammation. Immunotargets Ther. 2016:47–56. [PubMed: 27529061]
37. Alijotas-Reig J, Fernandez-Figueras MT, Puig L. Late-onset inflammatory adverse reactions related to soft tissue filler injections. Clin Rev Allergy Immunol. 2013:97–108. [PubMed: 23361999]
38. Ulijn RV, Bibi N, Jayawarna V, Thornton PD, Todd SJ, Mart RJ, Smith AM, Gough JE. Bioresponsive hydrogels. Mater Today. 2007:40–48.
39. Zhu J, Marchant RE. Design properties of hydrogel tissue-engineering scaffolds. Expert Rev Med Devices. 2011:607–626. [PubMed: 22026626]
40. Annabi N, Tamayol A, Uquillas JA, Akbari M, Bertassoni LE, Cha C, Camci-Unal G, Dokmeci MR, Peppas NA, Khademhosseini A. 25th Anniversary Article: Rational Design and Applications of Hydrogels in Regenerative Medicine. Adv Mater. 2014:85–124. [PubMed: 24741694]
41. Koshy ST, Ferrante TC, Lewin SA, Mooney DJ. Injectable, porous, and cell-responsive gelatin cryogels. Biomaterials. 2013
42. Verbeke CS, Mooney DJ. Injectable Pore-Forming Hydrogels for In Vivo Enrichment of Immature Dendritic Cells. Adv Healthc Mater. 2015:2677–2687. [PubMed: 26474318]
43. Kim JA, Lim J, Naren R, Yun HS, Park EK. Effect of the biodegradation rate controlled by pore structures in magnesium phosphate ceramic scaffolds on bone tissue regeneration in vivo. Acta Biomater. 2016:155–167.
44. Janik H, Marzec M. A review: fabrication of porous polyurethane scaffolds. Mater Sci Eng C Mater Biol Appl. 2015:586–591.
45. Murphy WL, Dennis RG, Kileny JL, Mooney DJ. Salt fusion: An approach to improve pore interconnectivity within tissue engineering scaffolds. Tissue Eng. 2002:43–52. [PubMed: 11886653]
46. Hou Q, Grijpma DW, Feijen J. Porous polymeric structures for tissue engineering prepared by a coagulation, compression moulding and salt leaching technique. Biomaterials. 2003:1937–1947. [PubMed: 12615484]
47. Miyazaki Y, Matsumoto N. Reduction of Intracranial Pressure with Fructose-Mannitol Solution. J Neurosurg. 1967:306–312. [PubMed: 6019737]
48. Sorani MD, Manley GT. Dose–response relationship of mannitol and intracranial pressure: a metaanalysis. J Neurosurg. 2008:80–87. [PubMed: 18173314]
49. Vegas AJ, Veiseh O, Doloff JC, Ma M, Tam HH, Bratlie K, Li J, Bader AR, Langan E, Olejnik K, Fenton P, Kang JW, Hollister-Locke J, Bochenek MA, Chiu A, Siebert S, Tang K, Jhunjhunwala S, Aresta-Dasilva S, Dholakia N, Thakrar R, Vietti T, Chen M, Cohen J, Siniakowicz K, Qi M,

McGarrigle J, Lyle S, Harlan DM, Greiner DL, Oberholzer J, Weir GC, Langer R, Anderson DG. Combinatorial hydrogel library enables identification of materials that mitigate the foreign body response in primates. Nat Biotechnol. 2016:345–352. [PubMed: 26807527]

50. Nahrendorf M, Swirski F. Monocyte and Macrophage Heterogeneity in the Heart. 2013
51. Delavary B, van der Veer WM, Egmond M, Niessen F, Beelen RHJ. Macrophages in skin injury and repair. 2011
52. Bury MI, Fuller NJ, Meisner JW, Hofer MD, Webber MJ, Chow LW, Prasad S, Thaker H, Yue X, Menon VS, Diaz EC, Stupp SI, Cheng EY, Sharma AK. The promotion of functional urinary bladder regeneration using anti-inflammatory nanofibers. Biomaterials. 2014:9311–9321. [PubMed: 25145852]
53. Schwartz M, Kipnis J, Rivest S, Prat A. How Do Immune Cells Support and Shape the Brain in Health, Disease, and Aging?. 2013
54. Tidball J, Wehling-Henricks M. Shifts in macrophage cytokine production drive muscle fibrosis. 2015
55. Tidball J, Dorshkind K, Wehling-Henricks M. Shared signaling systems in myeloid cell-mediated muscle regeneration. 2014
56. Swinehart IT, Badylak SF. Extracellular matrix bioscaffolds in tissue remodeling and morphogenesis. Dev Dyn. 2016:351–360. [PubMed: 26699796]
57. Brown BN, Londono R, Tottey S, Zhang L, Kukla KA, Wolf MT, Daly KA, Reing JE, Badylak SF. Macrophage phenotype as a predictor of constructive remodeling following the implantation of biologically derived surgical mesh materials. Acta Biomater. 2012:978–987. [PubMed: 22166681]
58. Dziki J, Badylak S, Yabroudi M, Sicari B, Ambrosio F, Stearns-Reider K, Turner N, Wyse A, Boninger ML, Brown E, Peter Rubin J. An acellular biologic scaffold treatment for volumetric muscle loss: results of a 13-patient cohort study. 2016
59. Medberry C, Crapo P, Siu BF, Carruthers CA, Wolf MT, Nagarkar SP, Agrawal V, Jones KE, Kelly J, Johnson SA, Velankar SS, Watkins S, Modo M, Badylak SF. Hydrogels Derived from Central Nervous System Extracellular Matrix. 2012
60. Sussman EM, Halpin MC, Muster J, Moon RT, Ratner BD. Porous implants modulate healing and induce shifts in local macrophage polarization in the foreign body reaction. Ann Biomed Eng. 2014:1508–1516. [PubMed: 24248559]
61. Blakney AK, Swartzlander MD, Bryant SJ. The effects of substrate stiffness on the in vitro activation of macrophages and in vivo host response to poly(ethylene glycol)-based hydrogels. J Biomed Mater Res A. 2012:1375–1386. [PubMed: 22407522]

Statement of significance

Our objective was to develop a fabrication process to create porous injectable hydrogels incorporating decellularized tissue digest material. This new hydrogel material was expected to exhibit faster cellular infiltration and a greater extent of pro-M2 macrophage polarization compared to control groups not incorporating each of the functional components. Poly(NIPAAm-co-VP-co-MAPLA) was chosen as the representative thermoresponsive hydrogel, and mannitol particles and digested urinary bladder matrix (UBM) were selected as the porogen and the bioactive decellularized material components respectively. In rat hindlimb intramuscular injection models, this new hydrogel material induced more rapid cellular infiltration and a greater extent of M2 macrophage polarization compared to control groups not incorporating all of the functional components. The hybrid hydrogel positively affected the wound healing outcomes of defects in rabbit adipose tissue with negligible inflammation and fibrosis, whereas scar formation and chronic inflammation were observed with autotransplantation and in saline injected groups.

The methodology of this report provides a straightforward and convenient mechanism to promote cell infiltration and mediate foreign body response in injectable hydrogels for soft tissue applications. We believe that the readership of *Acta Biomaterialia* will find the work of interest both for its specific results and general translatability of the findings.

All authors of this manuscript have seen and approved of this submission.

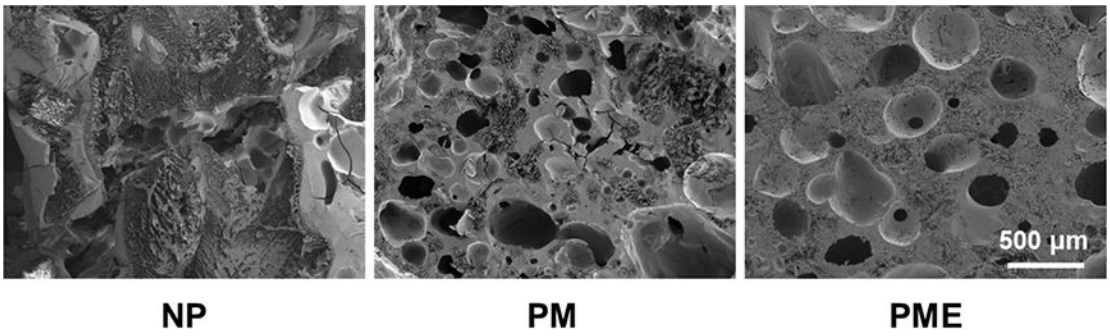

Figure 1.

Hydrogel cross-sections. NP: nonporous hydrogel, NPE: nonporous hydrogel without the UBM digest component, PME: porous hydrogel with the UBM digest component.

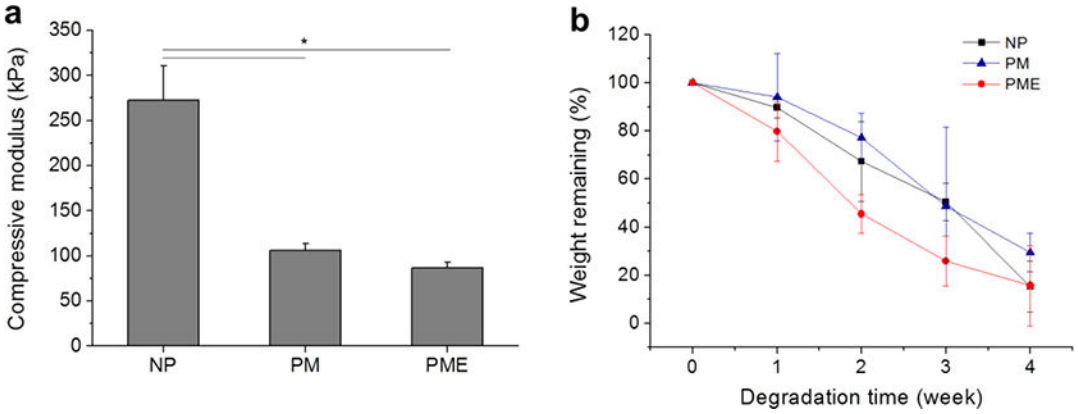

Figure 2.

(a) Compressive modulus of hydrogels. (b) Hydrogel degradation profile of hydrogels. * Significant difference, $p < 0.05$.

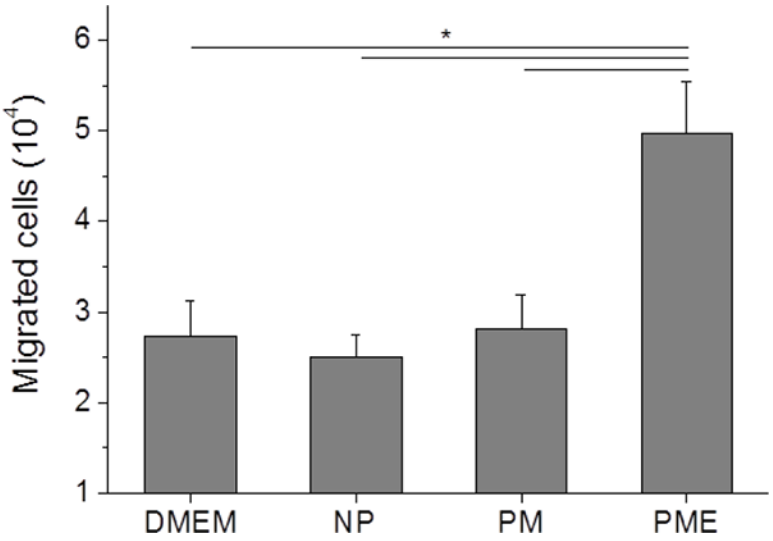

Figure 3.
Chemotactic migration of macrophage induced by release products from hydrogels.

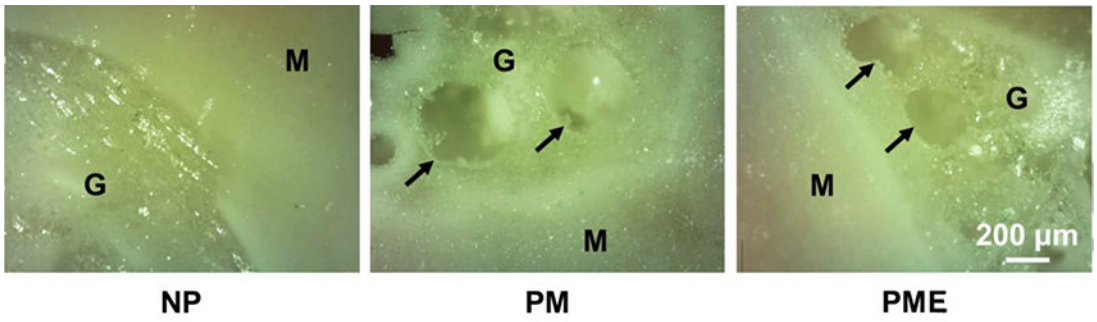

Figure 4.

In situ pore formation in hydrogels after intramuscular injections. M: muscle, G: hydrogel, Arrows: boundary of pores.

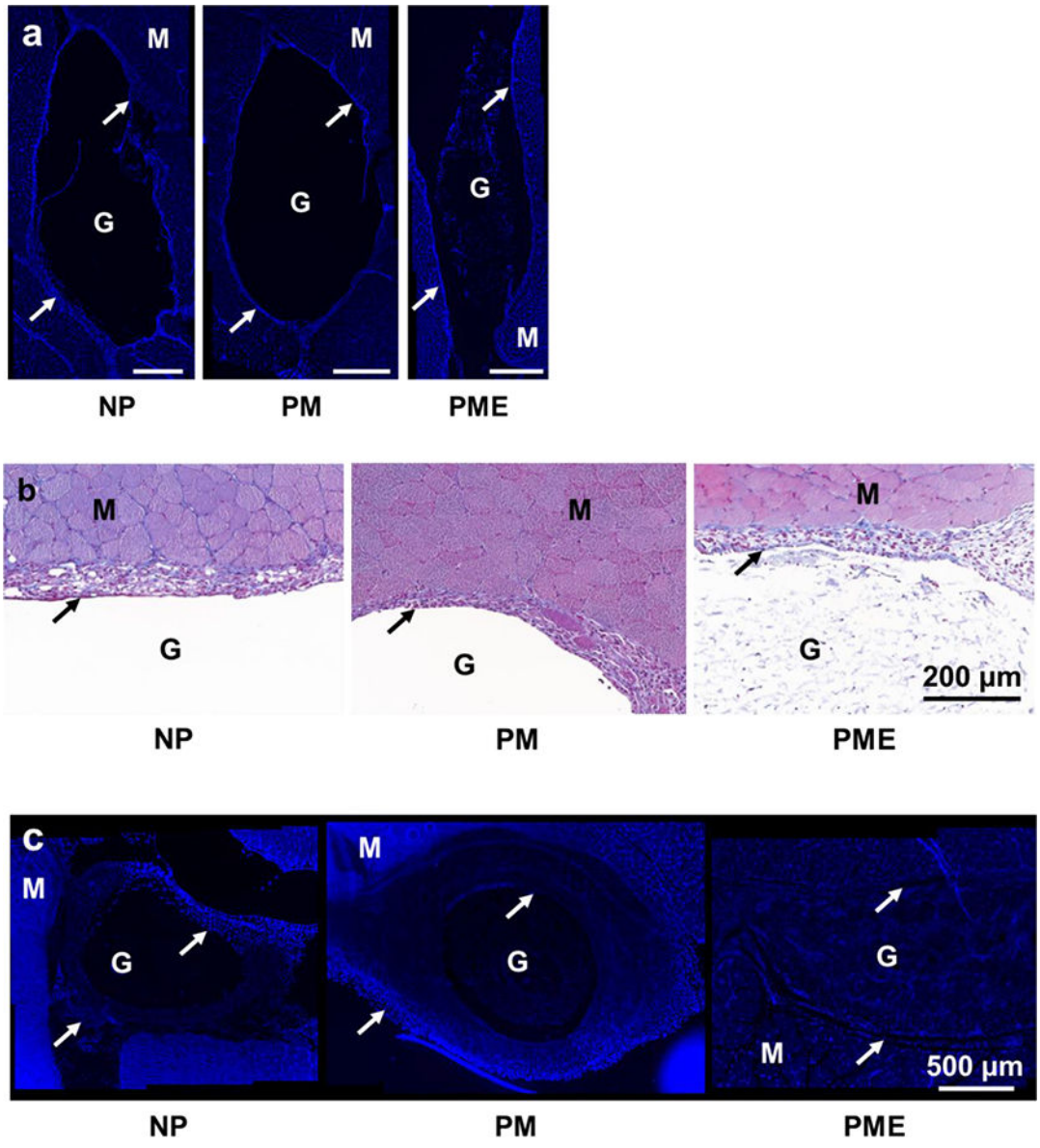

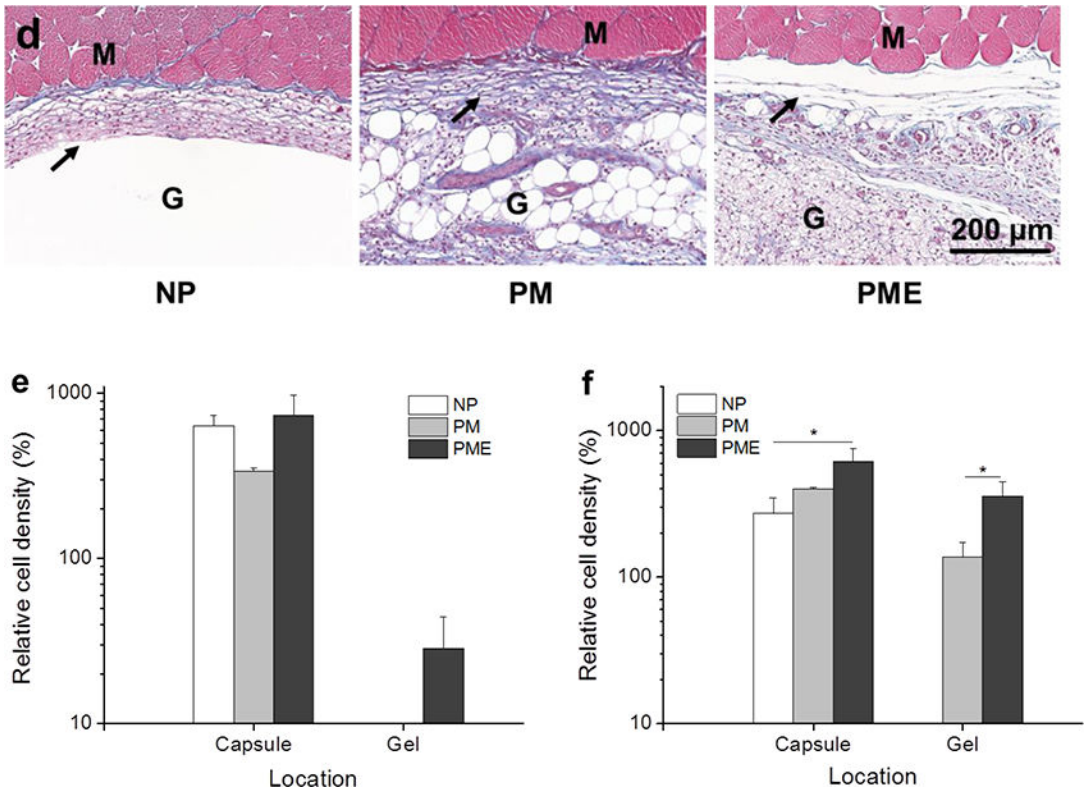

Figure 5.

Cell infiltration into injected hydrogels. M: muscle, G: hydrogel, Arrows: foreign body capsule. (a) DAPI staining of rat hindlimb muscle 3 days after hydrogel injection, scale bar = 500 μm. (b) Trichrome staining of rat hindlimb muscle 3 days after hydrogel injection. (c) DAPI staining of rat hindlimb muscle 21 days after hydrogel injection. (d) Trichrome staining of rat hindlimb muscle 21 days after hydrogel injection. (e,f) Relative cell density (muscle = 100%) in injected hydrogel and foreign body capsule 3 days and 21 days after injection.

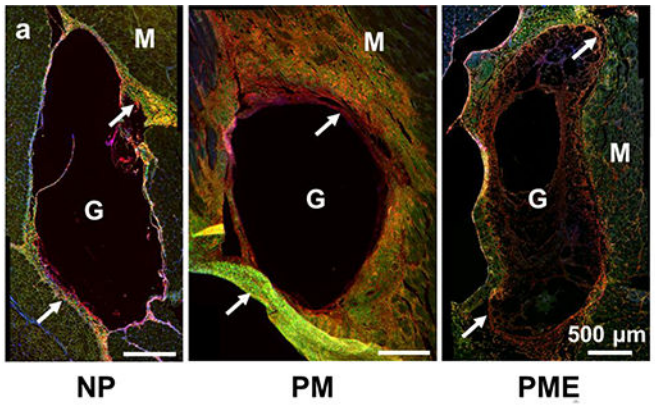

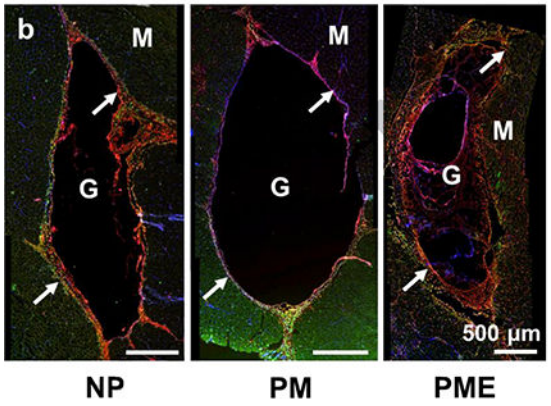

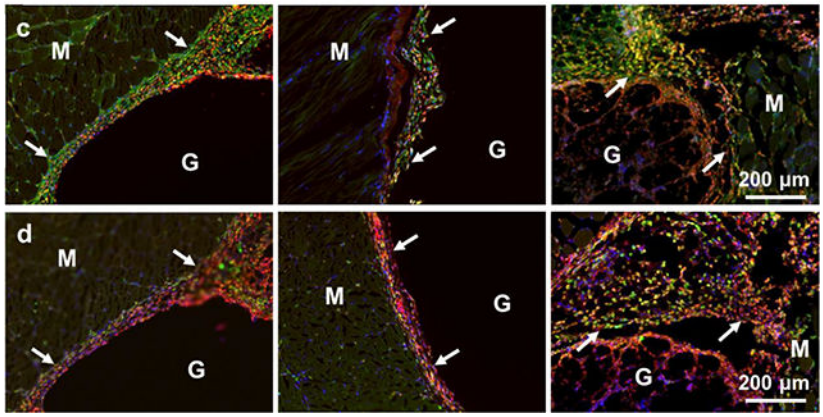

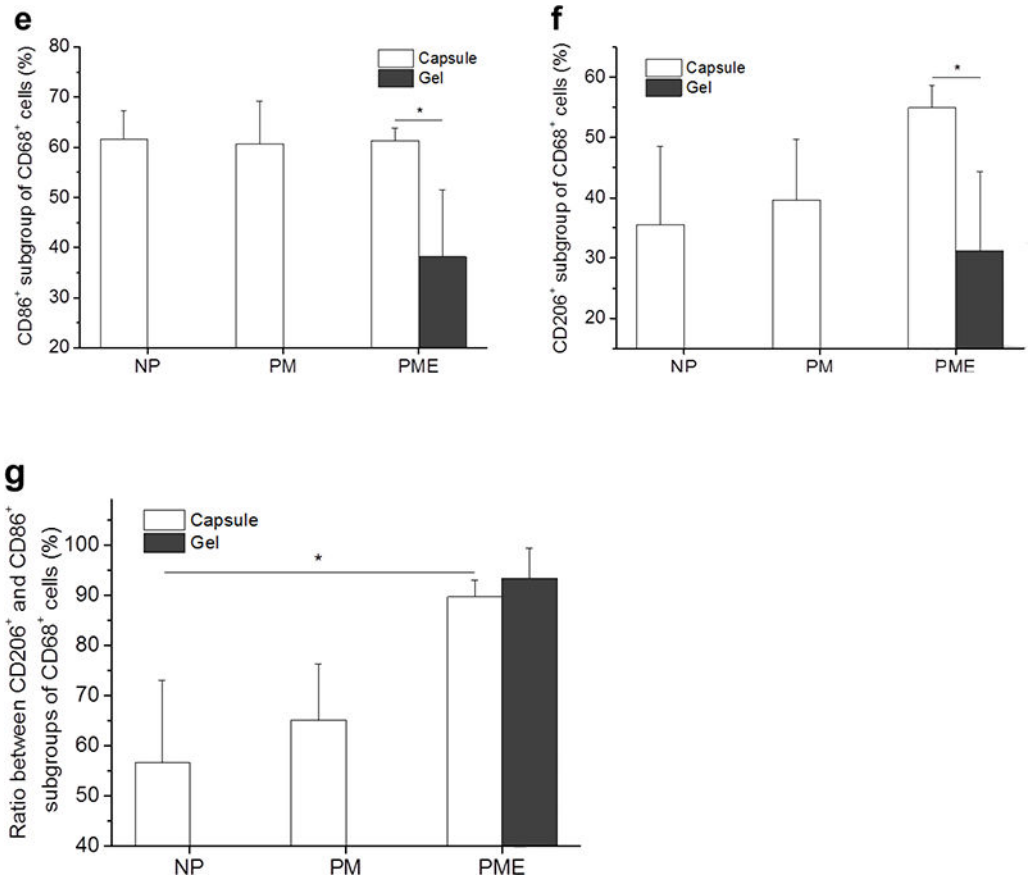

Figure 6.

Macrophage polarization 3 days after hydrogel injection. M: muscle, G: hydrogel, Arrows: foreign body capsule. (a) CD86 (green) and CD68 (red) staining. (b) CD206 (green) and CD68 (red) staining. (c) CD86 (green)/CD68 (red) and (d) CD206 (green)/CD68 (red) staining at the hydrogel/muscle interface. (e, f) Percentage of $CD86^+$ and $CD206^+$ cells in $CD68^+$ population, respectively. (g) Ratio between $CD86^+$ and $CD206^+$ cells in $CD68^+$ population. * Significant difference, $p < 0.05$.

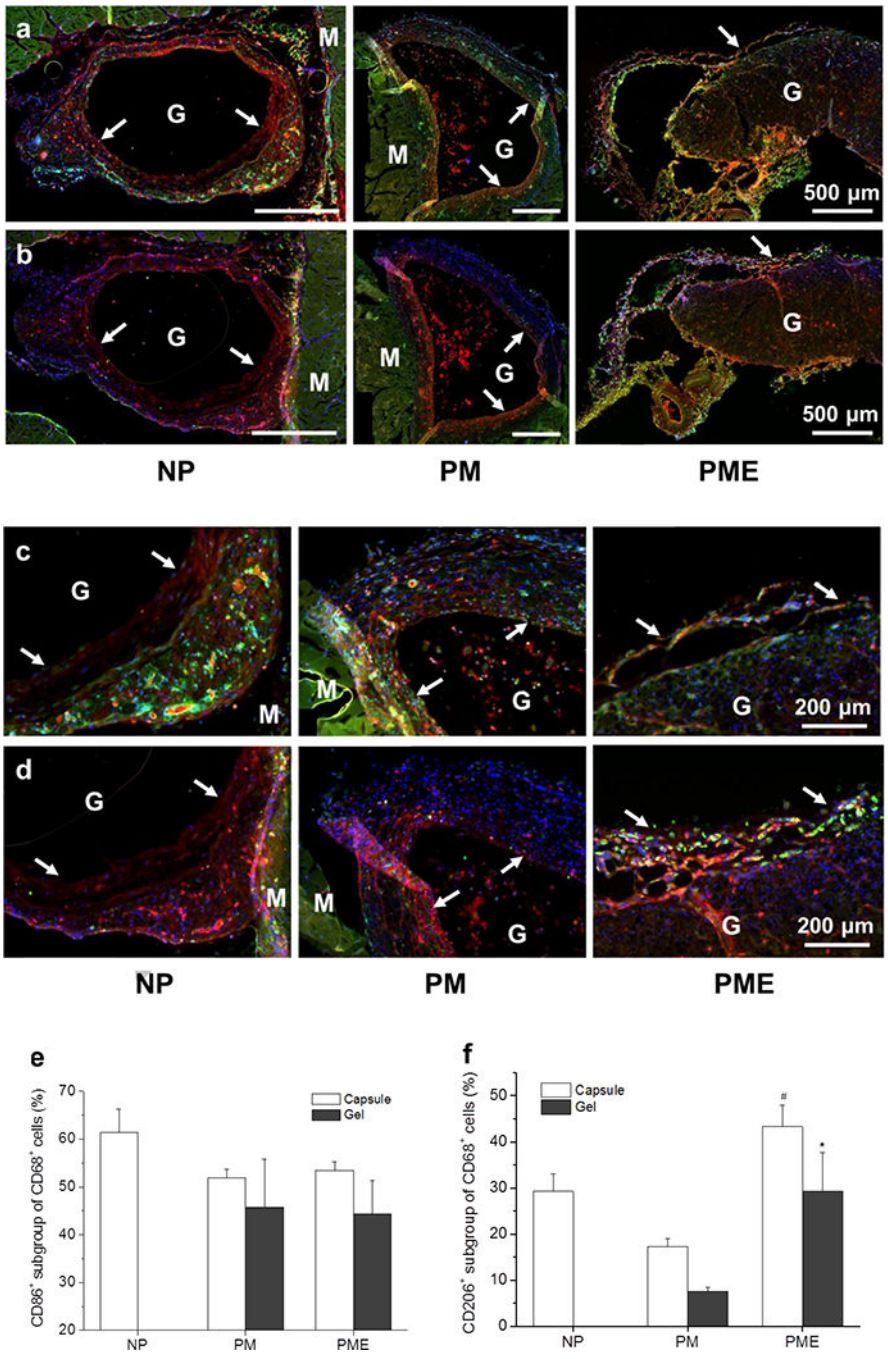

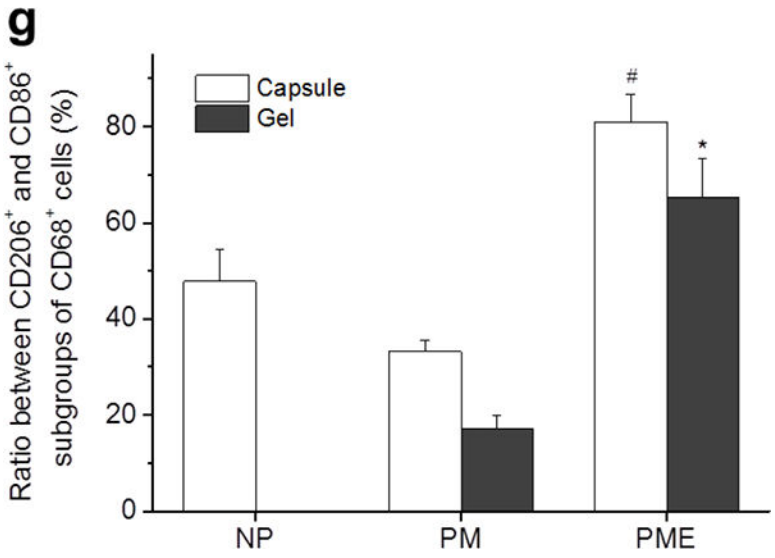

Figure 7.

Macrophage polarization in hydrogel injection sites after 21 days. M: muscle, G: hydrogel, Arrows: foreign body capsule. (a) CD86 (green) and CD68 (red) staining. (b) CD206 (green) and CD68 (red) staining. (c) CD86 (green)/CD68 (red) and (d) CD206 (green)/CD68 (red) staining at the hydrogel/muscle interface. (e, f) Percentage of $CD86^+$ and $CD206^+$ cells in $CD68^+$ population, respectively. (g) Ratio between $CD86^+$ and $CD206^+$ cells in $CD68^+$ population. * Higher than PM group, # Higher than NP and PM groups, $p < 0.05$.

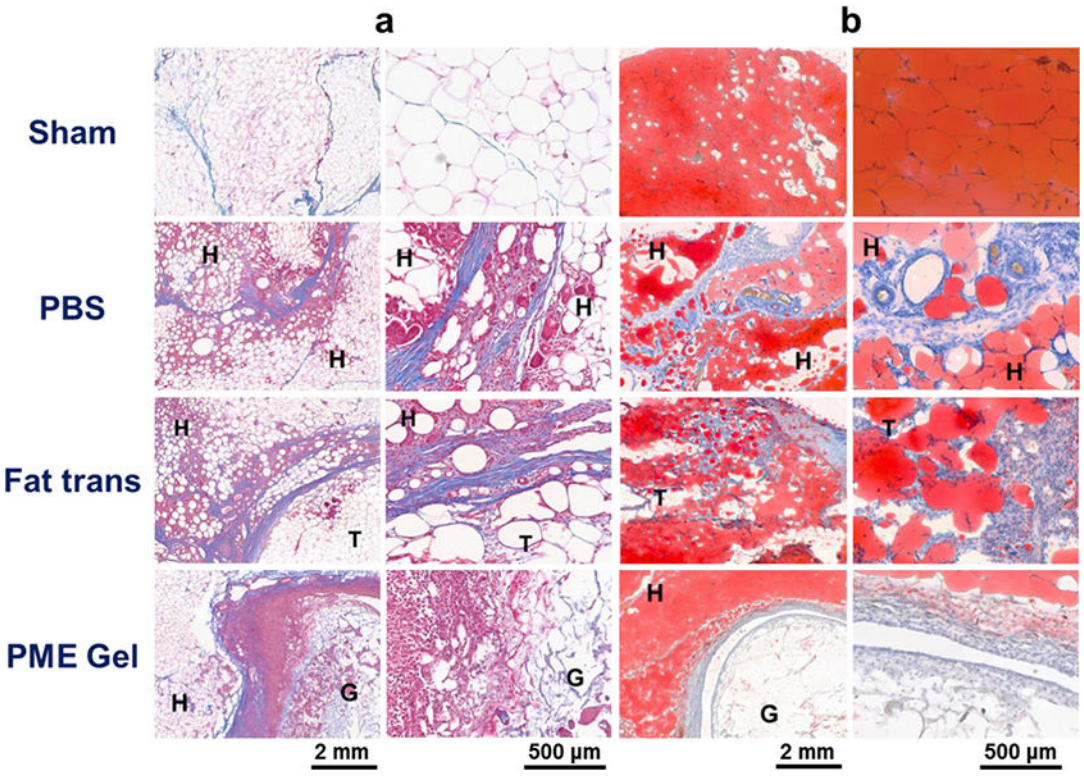

Figure 8.

Morphology of rabbit adipose tissue 2 weeks after treatment. H: healthy tissue, T: transplant. (a) Trichrome staining. (b) Oil Red staining.

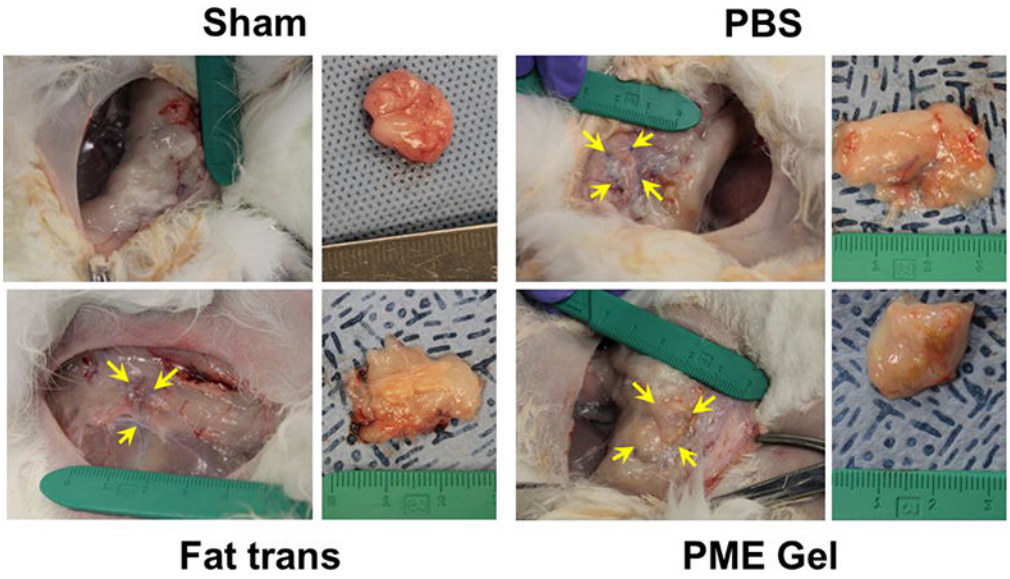

Figure 9.
Gross appearance of rabbit adipose tissue 8 weeks after treatment. Arrows: suture markers.

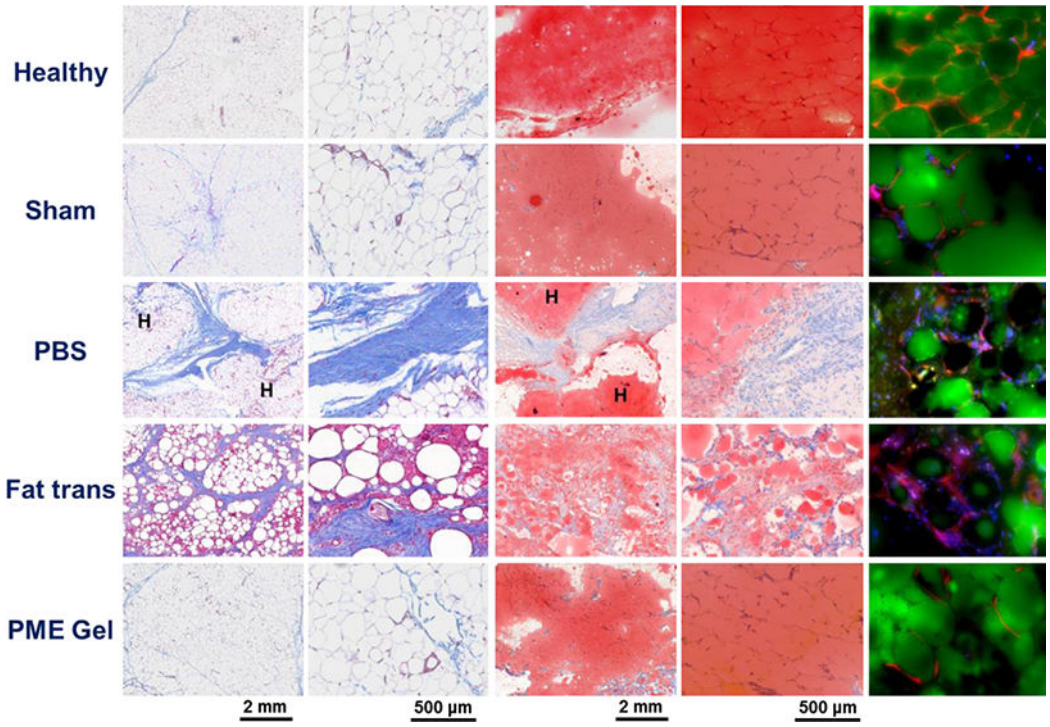

Figure 10.

Morphology of rabbit adipose tissue 8 weeks after treatment. H: healthy tissue. (a) Trichrome staining. (b) Oil Red staining. (c) Isolectin (red)/BIOPSY (green)/DAPI staining.

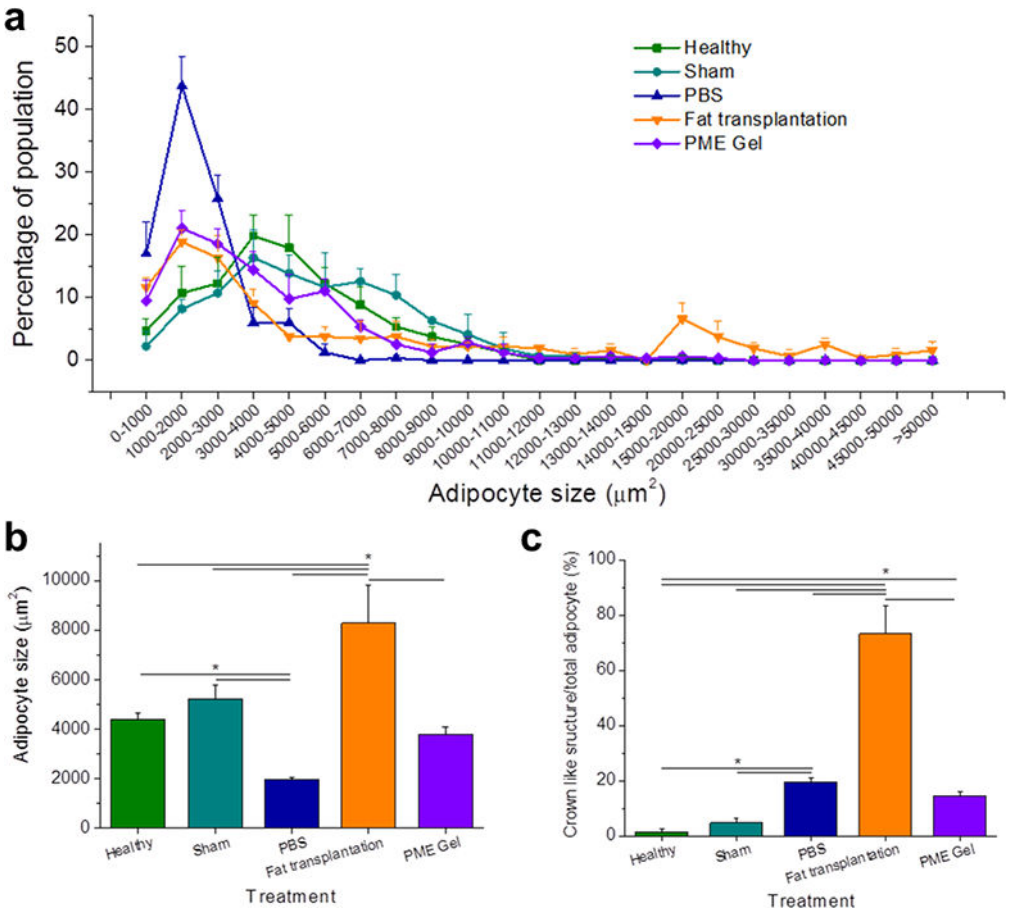

Figure 11.

Morphology analysis by adipocyte size and crown-like structure number. (a) Frequency distribution of adipocyte size. (b) Adipocyte size comparison among treatments. (c) Ratio between the quantity of crown-like structure and adipocytes. * Significant difference, $p < 0.05$.

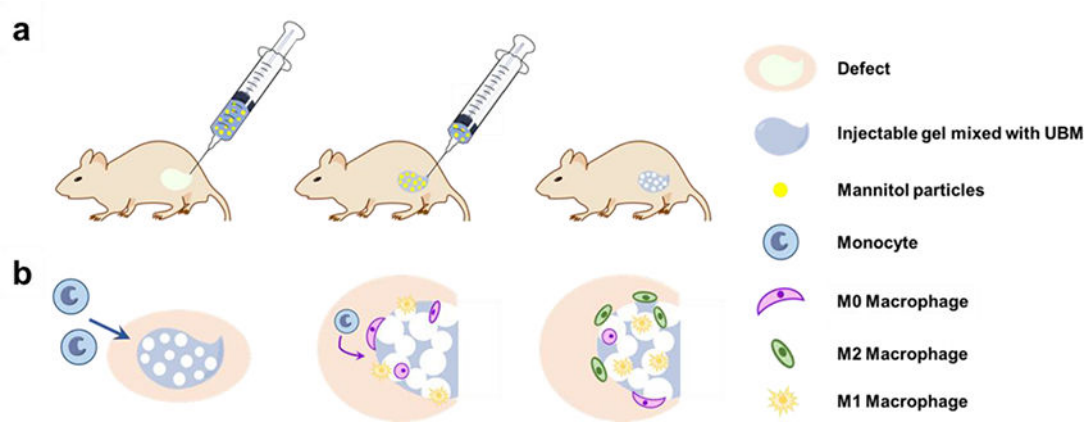

Scheme 1.

(a) In situ formation of pores immediately subsequent to hydrogel injection. (b) Faster cell infiltration and pro-M2 macrophage polarization in the porous injectable hydrogel.